



## Hydroxyapatite Biosynthesis by a *Serratia* sp. and Application of Nanoscale Bio-HA in the Recovery of Strontium and Europium

Rajkumar Gangappa, Ping Yong, Sarah Singh, Iryna Mikheenko, Angela J. Murray & Lynne E. Macaskie

To cite this article: Rajkumar Gangappa, Ping Yong, Sarah Singh, Iryna Mikheenko, Angela J. Murray & Lynne E. Macaskie (2016) Hydroxyapatite Biosynthesis by a *Serratia* sp. and Application of Nanoscale Bio-HA in the Recovery of Strontium and Europium, *Geomicrobiology Journal*, 33:3-4, 267-273, DOI: [10.1080/01490451.2015.1067657](https://doi.org/10.1080/01490451.2015.1067657)

To link to this article: <https://doi.org/10.1080/01490451.2015.1067657>



© 2016 Taylor & Francis Group, LLC



Published online: 04 Aug 2015.



Submit your article to this journal [↗](#)



Article views: 866



View related articles [↗](#)



View Crossmark data [↗](#)



Citing articles: 5 View citing articles [↗](#)

## Hydroxyapatite Biosynthesis by a *Serratia* sp. and Application of Nanoscale Bio-HA in the Recovery of Strontium and Europium

Rajkumar Gangappa, Ping Yong, Sarah Singh, Iryna Mikheenko, Angela J. Murray, and Lynne E. Macaskie

Unit of Functional Bionanomaterials, Institute of Microbiology and Infection, School of Biosciences, University of Birmingham, Edgbaston, Birmingham, United Kingdom

### ABSTRACT

A *Serratia* sp. expresses a high level of acid phosphatase when grown continuously under carbon limitation. In the presence of  $\text{CaCl}_2$ , biosynthesis of nanocrystalline hydroxyapatite (bio-HA) was achieved by utilizing phosphate released via enzymatic cleavage of an applied substrate (glycerol 2-phosphate: G2P). Hydroxyapatite crystals were identified by energy dispersive X-ray emission (EDX) and selected area diffraction (SAD). X-ray powder diffraction (XRD) analysis gave a mean crystallite size of  $\sim 21\text{--}32$  nm, with the smallest crystals (21–24 nm) obtained using 1 mM  $\text{Ca}^{2+}$  and 1 mM G2P. The uptake of  $\text{Eu}^{3+}$  and  $\text{Sr}^{2+}$  by bio-HA made by continuously pregrown cells (0.42 mg/mg and 0.043 mg/mg respectively) was  $\sim 20\%$  greater for  $\text{Sr}^{2+}$  than was previously reported for bio-HA material of size  $\sim 40$  nm made by batch-pregrown cells, while the corresponding uptake of  $\text{Eu}^{3+}$  was increased by  $> 1.8$ -fold. This was attributed to the localization of Eu (III) at grain boundaries by reference to previous work and highlights the potential of bio-HA as a sequestration agent for recovery of rare earth elements and trivalent actinides.

### ARTICLE HISTORY

Received June 2015  
Accepted June 2015

### KEYWORDS

Biomineralization;  
bioremediation; calcium  
phosphate; hydroxyapatite;  
*Serratia*

### Introduction

Hydroxyapatite (HA) is a major component of natural bone. Synthetic HA has been used widely in orthopaedics and dentistry (Gabriel et al. 2002; Vaz et al. 1999), while natural bone-HA has been used as a material for sequestering radionuclides (Dimovic et al. 2011). Studies to produce HA coated on metallic supports (Kameyama 1999; Keller and Dollase 2000; Tomsia et al. 1994) gave a thin HA film ( $\sim 40$  nm), which eventually peeled off (Kameyama 1999). By using a natural biofilm a biogenic coating of HA was obtained throughout the matrix of a 3-D structure (Macaskie et al. 2005). Use of biofilm yielded a highly adhesive biolayer (Yong et al. 2015), which was tightly held on a surface after HA-mineralization (Macaskie et al. 2005).


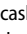
Attempts to make nanocrystalline HA have been reported by several authors (Beruto and Giordani 1999; Yeong et al. 2001), but the techniques were either energy demanding and/or yield limited. Biomineralization may be an alternative way to synthesise nanoscale-HA with potentially superior properties. Biofilm pre-grown under carbon-limitation was used to make HA (Macaskie et al. 2005); since this condition, and the biofilm format of growth, predominate in nature the ability of biofilm-cells to make HA suitable for entrapment of metallic ions was evaluated as the first step towards development of barriers for contaminated water flows.

A biofilm-forming *Serratia* sp. (NCIMB 40259) deposits metal ions as metal phosphates (Macaskie et al. 2000) mediated by the activity of a cell surface-located (Jeong et al. 1997) phosphatase (PhoN) to release precipitant phosphate from an

organic phosphate substrate e.g. glycerol 2-phosphate. The bacterial cells function both to “generate” inorganic phosphate and to provide nucleation sites for crystalline metal phosphate biomanufacture (Bontrone et al. 2000; Macaskie et al. 2000), with the extracellular/intercellular spaces of the cells used to ‘host’ crystals of metal phosphate enmeshed within extracellular polymeric materials (EPM).

This investigation focuses on the formation of cell-bound calcium phosphate crystals and identification of these as hydroxyapatite, with the aim to produce smaller crystallites than those obtained by “classical” methods including batch growth of bacteria shown previously (Handley-Sidhu et al. 2011a, 2011b). The rationale for this is that, since continuously pregrown cells produce copious extracellular polymers and since these polymers provide nucleation sites, cells pregrown under continuous culture should produce more, and hence smaller (for the same amount of  $\text{Ca}^{2+}$  provided) crystals than batch grown cells, while being stabilized against agglomeration by the surrounding EPM matrix. A previous study on the biodeposition of  $\text{NdPO}_4$  showed that, despite extensive biomineralization, an average crystallite size of  $\sim 14$  nm was obtained (Murray et al. 2015).

Biogenic HA (bio-HA) material has the ability to sequester metal ions effectively (Handley-Sidhu et al. 2011a, 2011b, 2014).  $\text{Sr}^{2+}$  and  $\text{Co}^{2+}$  both incorporate within the bulk inorganic amorphous phase, while  $\text{Co}^{2+}$  also incorporates within amorphous grain boundaries (Handley-Sidhu et al. 2014). However,  $\text{Eu}^{3+}$ , a surrogate for trivalent actinides, was taken

**CONTACT** Lynne E. Macaskie  l.e.macaskie@bham.ac.uk  Unit of Functional Bionanomaterials, Institute of Microbiology and Infection, School of Biosciences, University of Birmingham, Edgbaston, Birmingham B15 2TT, United Kingdom.

© 2016 Rajkumar Gangappa, Ping Yong, Sarah Singh, Iryna Mikheenko, Angela J. Murray, and Lynne E. Macaskie  
Published with license by Taylor and Francis

This is an open-access article distributed under the terms of the Creative Commons Attribution License <http://creativecommons.org/licenses/by/3.0/>, which permits unrestricted use, distribution, and reproduction in any medium, provided the original work is properly cited. The moral rights of the named author(s) have been asserted.

up only into the amorphous grain boundaries (Handley-Sidhu et al. 2014; Holliday et al. 2012). This suggests that a smaller crystallite size would confer a greater benefit for accumulating metals that bind at grain boundaries as compared to those that accumulate solely within the bulk amorphous phase due to the higher proportion of surface sites in smaller crystals. Hence, this study evaluates the potential for the use of continuously pregrown bacteria for the production of bio-HA since previous studies (Murray et al. 2015) showed that cells grown in this way made crystallites of  $\text{NdPO}_4$  of size  $\sim 14$  nm.

Continuous radionuclide decontamination is possible by use of biofilm-immobilized host mineral as a filter. This approach was pioneered for the removal of  $^{90}\text{Sr}^{2+}$  and  $^{137}\text{Cs}^+$  from a nuclear reactor waste via use of biogenic uranium phosphate as the 'host' biomineral (Paterson-Beedle et al. 2006). Since the waste contained natural uranium the use of a uranium-biomaterial was acceptable. However contemporary challenges such as the Fukushima accident and the resulting clean up operations, as well as the large extent of 'legacy' contaminations worldwide, have highlighted the need for cheap, scalable, non-toxic and robust solutions for radionuclide removal from contaminated soils and waste waters and an earlier study evaluated this potential for  $\text{Sr}^{2+}$  removal (Handley-Sidhu et al. 2011b).

However, in addition to being a convenient actinide "surrogate,"  $\text{Eu}^{3+}$  is a valuable element within the group known as rare earth elements (REEs) for which effective routes to recovery are urgently sought to mitigate the current monopoly (> 95%) of the REE global supply by China. REEs are essential to many modern technologies (Murray et al. 2015) but their refining is complex. Because bio-HA was shown to accumulate  $\text{Eu}^{3+}$  (Holliday et al. 2012) this approach was extended in this study to evaluate the scope for using nanocrystalline bio-HA as a capture agent for  $\text{Eu}^{3+}$  with a view to the potential recovery of REE from wastes.

## Materials and methods

### Biomass preparation

*Serratia* NCIMB 40259 was cultured under carbon (lactose)-limited continuous condition at 28–30 °C in an airlift fermenter

as described previously (Macaskie et al. 2005). The culture was started by the addition of 100 ml inoculum, which had been pre-grown in similar medium. After 24h growth batchwise ( $\text{OD}_{600} \sim 0.6$ ) the fermenter was switched to continuous mode (flow rate:  $\sim 210$  ml/h), and maintained at steady-state (Macaskie et al. 2005). Culture outflow was retained, harvested by centrifugation and washed in isotonic saline ( $8.5 \text{ g l}^{-1}$  of NaCl) and stored at 4 °C until use.

The culture was monitored by measurement of phosphatase activity and cell density in the fermenter outflow (Macaskie et al. 2005). Phosphatase activity was assayed by the release of *p*-nitrophenol (PNP) from *p*-nitrophenyl phosphate (PNPP) as described previously (Macaskie et al. 2005). This investigation focussed on the bio-HA produced by planktonic cells. Biofilms were also made in parallel by incorporation of polyurethane reticulated foam supports within the vessel (Macaskie et al. 2005; Murray et al. 2015). The biofilms were retained for later work to evaluate the use of immobilised biofilm-HA in a subsequent investigation.

### Bioaccumulation of calcium phosphate by *Serratia* NCIMB 40259 cells with dosed additions of $\text{Ca}^{2+}$ , G2P and citrate

For the synthesis of hydroxyapatite, flasks containing usually 100 ml of TAPSO/NaOH buffer (50 mM, pH 8.6, 9.2 or 7.0;  $\text{pK}_a$  at 25 °C is 7.60) and *Serratia* sp. (resuspended to  $\text{OD}_{600} = 1.0$ ) were dosed daily with various concentrations of  $\text{CaCl}_2$ , trisodium citrate and glycerol 2-phosphate (G2P) as shown in Table 1. Flasks were incubated at 30 °C on a shaker (120 rpm). Bio-hydroxyapatite (bio-HA) was harvested after 8 days by centrifugation, washed twice in distilled  $\text{H}_2\text{O}$ , air dried, then manually ground. Hydroxyapatite (HA) type -1 (Sigma, EC No 215-145-7) was used for comparison in XRD studies.

### Examination of cell-bound deposits using electron microscopy

Calcium phosphate loaded cells that had been challenged with eight daily additions (1 mM  $\text{Ca}^{2+}$ , 5 mM G2P, with and without 2mM citrate), were fixed with 2.5% glutaraldehyde (in

**Table 1.** Bio-hydroxyapatite samples made in this study.

Samples	Substrate Concentrations (mM)			*Dry weight of bio-HA synthesized (mg/100ml)	XRD Crystallite size (nm)
	Na-Citrate	$\text{CaCl}_2$	G2P		
pH 9.2					
9.2A	2	2	5	235	25
9.2B	2	1	5	136	26
9.2C	0	2	5	245	26
9.2D	0	1	5	137	25
9.2E	2	1	1	146	24
pH 8.6					
8.6A	2	2	5	248	32
8.6B	2	1	5	130	24
8.6C	0	2	5	231	27
8.6D	0	1	5	140	25
8.6E	2	1	1	136	22
pH 7	2	1	1	111	21

\*Errors (Standard error of the mean) were generally within 5% of the mean throughout. Bio-HA was synthesized as described in Materials and Methods with daily additions as shown (the dose volume was adjusted to accommodate increasing volumes or decreased volumes where samples were removed to check for complete removal of  $\text{Ca}^{2+}$ ). Dry weight of bio-HA obtained/100 ml is shown (biomass dry weight was  $\sim 50$  mg/100 ml suspension).

0.1 M Na cacodylate/HCl buffer pH 5.2) at 4°C for 1 h. For scanning electron microscopy samples were dehydrated at ambient temperature, coated with carbon, and examined under High-Vacuum Mode on an environmental scanning electron microscope (ESEM: FEI Philips FEG ESEM XL30, SEM Detector: 15 kV). For transmission electron microscopy (TEM) sectioned samples were osmium-stained, and examined under a transmission electron microscope (TEM: JEOL JEM-1200EX Electron Microscope, 80 kV). Selected area diffraction (SAD) patterns were obtained at high resolution.

### Characterization of bio-HA by X-ray powder diffraction

The samples were laid onto a silicon crystal plate and analyzed using a high precision X-ray powder diffractometer (Bruker D8 diffractometer, School of Chemistry, University of Birmingham) for data collection. The powder diffraction patterns were recorded from 20° to 70° (2θ) with a step length of 0.05° (2θ). The average crystallite size of the materials was calculated by using Scherrer's equation (Ledo et al. 2008).

### Use of bio-HA for metal uptake from aqueous solutions

Solutions of Sr(NO<sub>3</sub>)<sub>2</sub> and Eu(NO<sub>3</sub>)<sub>3</sub> were prepared in dH<sub>2</sub>O (≤15.0 MΩ/cm) to give final concentrations of 0.5 mM (pH 5–6). All sorption experiments were carried out in triplicate. The ability of bio-HA made at pH 7.0 (Table 1) to scavenge Sr<sup>2+</sup> and Eu<sup>3+</sup> was tested by suspending ~10 mg of bio-HA in 100 ml of 0.5 mM Sr(NO<sub>3</sub>)<sub>2</sub> or Eu(NO<sub>3</sub>)<sub>3</sub>. The preparations were shaken at room temperature (150 rpm). At intervals (0.5, 2, 5, 24, and 51 h) samples were harvested by centrifugation. Residual Eu<sup>3+</sup> in supernatants was measured by mixing 1.97 ml of 1M ammonium acetate buffer (pH 3.3) with 30 μl of supernatant; Eu<sup>3+</sup> was visualized by adding 0.15% w/v (aq.) arsenazo (III). The pink complex was measured at 652nm and the Eu<sup>3+</sup> concentration was estimated by reference to a standard curve, similarly prepared. Residual Sr<sup>2+</sup> (and Ca<sup>2+</sup> released from bio-HA) was measured in sample supernatants using Inductively Coupled Plasma-Optical Emission Spectroscopy (ICP-OES; Agilent 7500ce; University of Plymouth, UK). Phosphate was assayed as described previously (Murray et al. 2015).

## Results

### Scanning and transmission electron microscopy

Examination by SEM of calcium phosphate-loaded cells shows that, without citrate, the precipitate appeared diffuse (Figure 1A), whereas that made with citrate appeared more dense (Figure 1B). Cells without Ca<sup>2+</sup> showed no precipitate (Figures 1C and 1G). Figure 1A shows the needle-like crystals, which are characteristic of hydroxyapatite. A similar pattern was seen using TEM examination where the depositions appear to be denser and larger when made in the presence of citrate (Figures 1B, 1F). Without citrate, Ca<sup>2+</sup> would be at a higher free concentration in solution and hence calcium phosphate would precipitate rapidly on the outside of the cells, giving regular, needle-like HA crystals (Durucan and Brown 2000). No

precipitation was detected for more than 8 days using cell-free controls and analysis of the solution confirmed no loss of Ca<sup>2+</sup>.

### EDX and selected area diffraction analysis (SAD)

The ratios of Ca/P were determined for the bio-precipitates made from solution with or without citrate using EDX (Figure 1D), and were 1.67 ± 0.11 (n = 10) and 1.65 ± 0.09 (n = 10) for precipitates made with and without citrate respectively, compared to 1.67 for the Ca/P ratio of HA (Ca<sub>5</sub>(PO<sub>4</sub>)<sub>3</sub>OH); all were identical within experimental error. Selected area diffraction analysis (SAD) under TEM (Figure 1H) gave d-spacing values from the SAD pattern (D<sub>1</sub>: 3.44Å and D<sub>2</sub>: 2.81Å) associated with the strong diffraction rings of HA (002), (211) (Anonymous 1992). The bio material was concluded to be hydroxyapatite.

### X-ray powder diffraction (XRD)

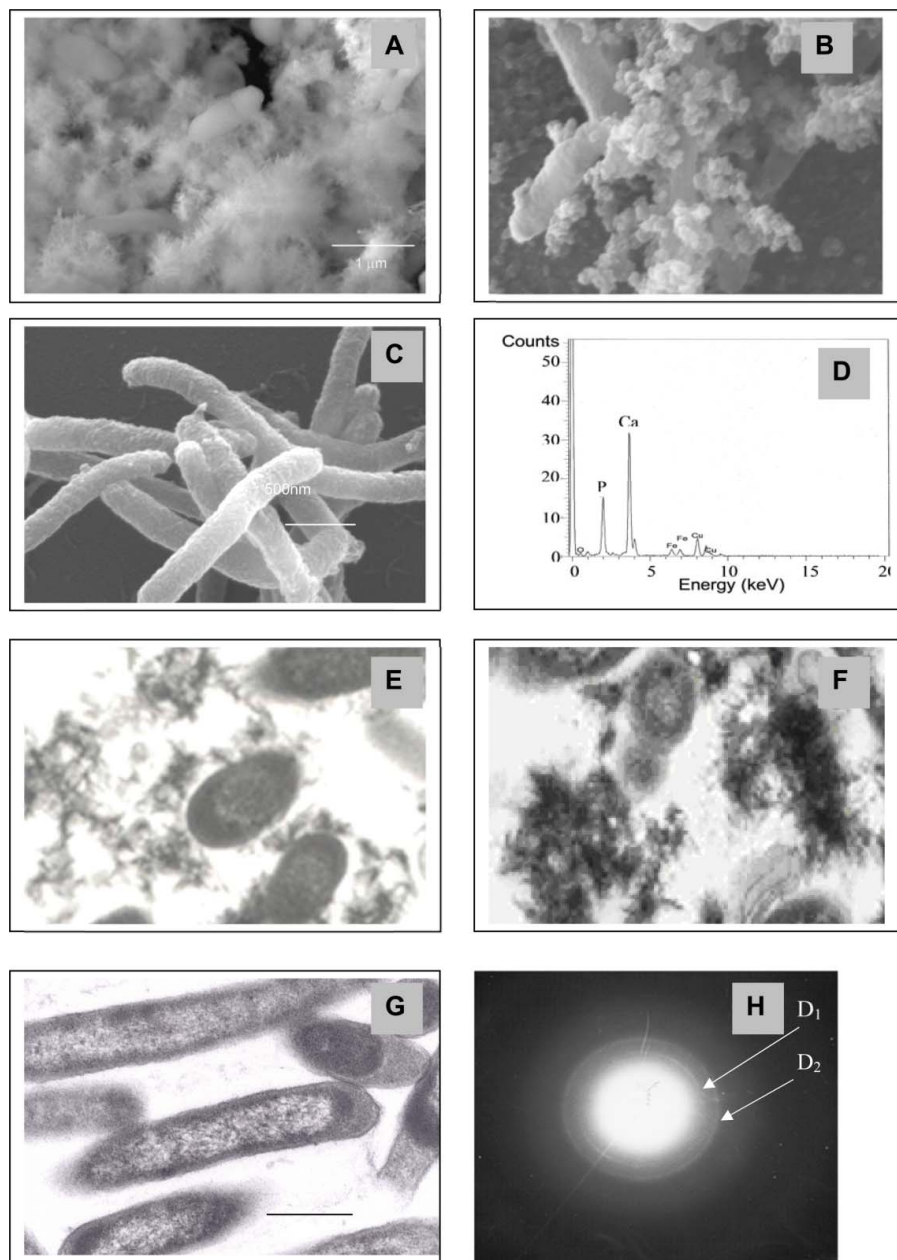
The XRD powder patterns obtained for the bio-HA synthesized under various conditions (Table 1) are shown in Figure 2A. The peak positions were matched against commercial hydroxyapatite, confirming that the synthesized biomineral was HA. The less well defined and broader bio-HA peaks are indicative of nanocrystallites or of an amorphous nature. The average crystallite size was estimated by using Scherrer's equation, giving sizes ranging from 24 to 26 nm (made at pH 9.2), 22 to 32 nm (at pH 8.6) and 21 nm in samples made at pH 7.0 (Table 1 and Figure 2B). Accurate measurement is difficult due to the broad nature of the XRD peaks of nanomaterials.

The smallest crystallite sizes were obtained by reducing the G2P concentration from 5 mM to 1 mM in samples made at pH 8.6 and 7.0 (Figure 2B) and since use of glycerol 2-phosphate is costly 1 mM was adopted in further work. The samples selected for further study were those made at pH 7 (Table 1). The HA mineral component was calculated to comprise ~50% of the total mass of the material (by reference to a known OD<sub>600</sub>/dry weight calibration and a known amount of cells used: see Methods), i.e., equivalent to 100% of the bacterial dry weight.

### Metal uptake by Bio-HA

The uptake of Eu<sup>3+</sup> and Sr<sup>2+</sup> by bio-HA is shown in Figures 3A and 3B. Sorption of both metal ions was rapid during 30 min of incubation. Further incubation showed no significant increase in Sr<sup>2+</sup> uptake (Figure 3B), whereas increased uptake of Eu<sup>3+</sup> was observed up to 24 h (Figure 3A). Eu<sup>3+</sup> uptake (~42 mg/100 mg bio-HA; ~0.84 mg/mg HA mineral) was ~10 times higher than for Sr<sup>2+</sup> (~4.3 mg/100 mg bio-HA; ~0.086 mg/mg HA), i.e., on a molar basis approximately 5-fold greater uptake of Eu<sup>3+</sup> was obtained (atomic weights of Eu and Sr are 152 and 87.6, respectively). Negligible Ca<sup>2+</sup> or phosphate was detected in the residual solutions, i.e., negligible dissolution of the HA occurred. Tests were also done using material made at pH 8.6 with similar results.





**Figure 1.** Scanning (A-D) and transmission (E-H) electron microscopy of *Serratia* cells following accumulation of calcium phosphate. Cells were examined by SEM and TEM following deposition of calcium phosphate from solution containing 1 mM Ca<sup>2+</sup> and 5 mM glycerol 2-phosphate. Results were similar at all pH values and representative examples are shown. Magnifications are as shown. A, E: cells with calcium phosphate precipitated from solution without citrate. B, F: cells with calcium phosphate precipitated from solution with citrate. C, G: Controls (cells unsupplemented with Ca<sup>2+</sup> and G2P). Bars are 1 μm. D: Energy dispersive X-ray emission (EDX) under environmental scanning electron microscopy (SEM mode) for A and B. H: Selected area diffraction (SAD) of areas of electron opaque material in E and F: the d-spacing values of the SAD pattern were (D<sub>1</sub>: 3.44 Å and D<sub>2</sub>: 2.81 Å) associated with strong diffraction rings of HA (002), (211) (JCPDS file 09-0432).

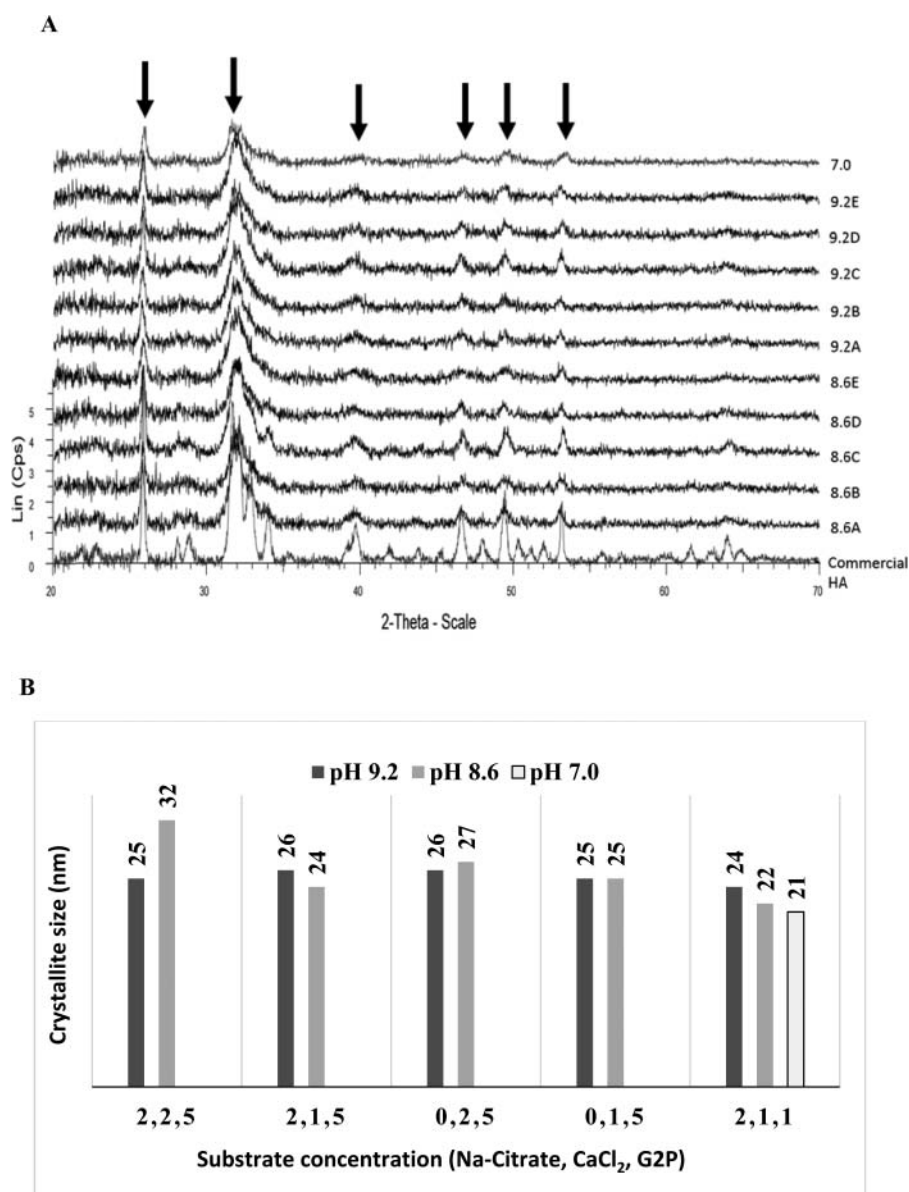
## Discussion

### *Biosynthesis of hydroxyapatite nanocrystals by Serratia sp.*

When cells are challenged with Ca<sup>2+</sup> and G2P, the biomineralization process relies on the cellular microenvironment becoming supersaturated with inorganic phosphate released from G2P within a structured exocellular space dominated by the extracellular polymeric matrix. The initial event in metal phosphate precipitation is the formation of a complex between incoming metal and phosphate groups on the cellular lipopolysaccharide (LPS). Ferris and Beveridge (1984) noted that LPS,

containing substantial phosphorus, occurred in outer-membrane vesicles and these showed metal-binding ability.

Bonthrone et al. (2000) and Macaskie et al. (2000) used <sup>31</sup>P NMR to confirm this as a metal phosphate nucleation mechanism. Another study described the production of extracellular membrane vesicles rich in LPS which served as an export mechanism for alkaline phosphatase (Kadurugamuwa and Beveridge 1995). Hence, assuming that the acid phosphatase (PhoN) is exported in a similar way the LPS would have a dual role in both the localization of the phosphatase (“tethering” this within the exocellular material) and also being the focus for metal phosphate nucleation.



**Figure 2.** (A) X-ray powder diffraction analysis of samples. XRD powder patterns for various bio-HA samples as shown in Table 1. A commercial HA sample is shown for reference. (B) Crystallite size of bio-HA nanoparticles synthesized in varied pH and substrate concentrations. Crystallite sizes were calculated from the peaks arrowed. Sample notation: see Table 1.

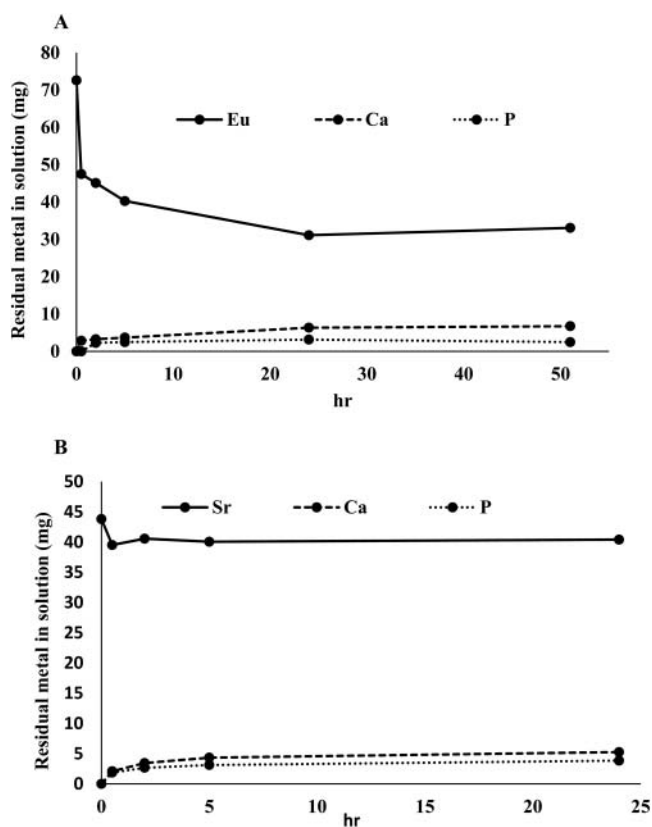
Nucleation represents an activation energy barrier to the spontaneous formation of a solid phase from a supersaturated solution. For 1 mM free Ca<sup>2+</sup> in bulk solution without complexing reagent, by calculation, precipitation should occur for CaHPO<sub>4</sub> at 0.1 mM HPO<sub>4</sub><sup>2-</sup> ( $K_{sp} = 1 \times 10^{-7}$  for CaHPO<sub>4</sub>; Dean 1992) but this would be promoted in a local phosphate-rich environment and also by an alkaline pH where free PO<sub>4</sub><sup>3-</sup> would predominate. The effect of citrate was to extend the delay before onset of Ca<sup>2+</sup> precipitation to 2 days, following which the results obtained with and without citrate were similar. The morphology of the crystallites appeared to be different in the presence and absence of citrate (Figures 1A, 1B) but with little effect on the overall crystallite size (Table 1).

Overall, the HA yields with and without citrate were similar. Small bio-HA nanoparticles were obtained by daily dosing with 1 mM CaCl<sub>2</sub> and 1 mM G2P regardless of the pH (pH 9.2, 8.6 or 7.0). As suggested by Handley-Sidhu et al. (2014) smaller

nanoparticles have a larger surface area and hence would show enhanced uptake of metals that bind at the NP surface but with less enhancement for metals that locate throughout the crystal structure. For the purpose of establishing the ability of the material to take up Eu<sup>3+</sup> and Sr<sup>2+</sup> a HA loading of ~100% of the bacterial dry weight was selected (50 mg cells with ~ 50 mg HA) although the HA deposition in samples with 2 mM Ca<sup>2+</sup> and 5 mM G2P extended to more than twice this level (Table 1) without major adverse effect on the crystallite size (Table 1; Figure 2B).

#### **Uptake of Eu<sup>3+</sup> and Sr<sup>2+</sup> into Bio-hydroxyapatite**

Handley-Sidhu et al. (2011a, 2011b, 2014), previously showed that *Serratia* bio-HA has an enhanced capacity for divalent and trivalent metal sorption when compared to a commercially synthesized counterpart. However, these tests used cells pregrown



**Figure 3.** (A)  $\text{Eu}^{3+}$  uptake by 100 mg bio-HA (measured colorimetrically) and calcium and phosphorus leaching from 100 mg bio-HA. (B)  $\text{Sr}^{2+}$  uptake by 100 mg bio-HA, measured by ICP-OES. Calcium and phosphorus leaching from 100 mg bio-HA. Solid lines:  $\text{Eu}^{3+}$  and  $\text{Sr}^{2+}$  removal. Dashed lines: release of  $\text{Ca}^{2+}$ . Dotted lines: release of phosphate. Errors (SEM) were generally within 5% of the mean throughout.

in batch culture, with a mean particle size of 40 nm. In this study nanoscale bio-HA made by continuously-pregrown cells was examined using material made at pH 7.0 with 1 mM  $\text{CaCl}_2$ , 1 mM G2P and 2 mM Na-citrate (crystallite size  $\sim 21$  nm, i.e., approximately 1/2 of the value previously reported). The uptake of metal ions by this bio-HA showed  $\text{Eu}^{3+}$  uptake ( $\sim 42$  mg/100 mg of bio-HA) to be  $\sim 10$  times higher than that of  $\text{Sr}^{2+}$  ( $\sim 4.3$  mg/100 mg bio-HA) on a mass basis (i.e.,  $\sim 5$  times higher on a molar basis) which corresponded to 43 wt% loading of Eu (III) into bio-HA (or 86% of the mass of the HA mineral component), but only  $\sim 4.3$  wt% of Sr ( $\sim 8\%$  of the HA mineral component). These correspond to an uptake increased by 180% and  $\sim 20\%$  for  $\text{Eu}^{3+}$  and  $\text{Sr}^{2+}$  respectively, as compared to earlier results using 40 nm bio-HA material (Handley-Sidhu et al. 2014).

These findings corroborate previous reports regarding the different mechanisms of uptake and incorporation of the metal ions (Handley-Sidhu et al. 2011; Holliday et al. 2012; Handley-Sidhu et al. 2014). Sr (II) locates within the bulk amorphous phase, while Eu (III) locates at the grain boundaries. Hence the smaller HA-crystallite size produced using continuously pre-grown cells in this study is the likely factor responsible for the nearly doubled sorption ability via the ensuing higher surface area of the HA; smaller crystallites would be expected to increase the uptake of  $\text{Eu}^{3+}$  but not  $\text{Sr}^{2+}$ , since the former is

confined to grain boundaries, i.e., a surface phenomenon (above). The relative surface areas of spheres of diameter 21 and 40 nm would be 1385 and 5027  $\text{nm}^2$ , i.e., the nominal capacity for Eu(III) could be increased by 3.6 times by using smaller spherical NPs. However, as shown in Figures 1A and 2, the biomaterial comprised needle-shaped crystals and the aspect of these nanocrystals, as well as their degree of separation from each other, may also play a role.

The role of the biological residue in the biomineral sample should not be ignored. Biological residue containing an excess of residual extracellular polymer matrix (EPM) may play a role in stabilizing the HA crystals against agglomeration or overgrowth and, indeed, bacteria heavily loaded with macroscopic amounts of  $\text{NdPO}_4$  still showed a mean crystallite size of  $\sim 14$  nm (Murray et al. 2015). Since bio-HA in the current study shows a higher capacity for  $\text{Eu}^{3+}$  than that described previously (Handley-Sidhu et al. 2014) this suggests that the recovery of  $\text{Eu}^{3+}$  (but only marginally that of  $\text{Sr}^{2+}$ ) can be enhanced by the choice of cell pregrowth method; the use of carbon-limiting continuous culture may approximate to the condition where a mineral barrier might be expected to form naturally using natural biofilms.

Overall this study indicates that the bio-HA is an efficient material for recovery of  $\text{Eu}^{3+}$  from aqueous solution. Confirmation that this is attributable to a surface area phenomenon is in progress. If, indeed, the presence of EPM facilitates the persistence of small HA nanocrystallites under heavy loading then the use of immobilized biofilm-HA as an agent for high yield recovery of  $\text{Eu}^{3+}$  is feasible and this has been shown using biofilms that were made in parallel within this study; the immobilized biomaterial functioned for many weeks in the continuous removal of  $\text{Eu}^{3+}$  (A. J. Murray and S. Singh, unpublished). These results will be reported in full in a later publication

## Conclusions

The crystallite size of bio-hydroxyapatite can be reduced by use of continuously pre-grown cells. Small HA-nanocrystallites ( $\sim 21$ – $24$  nm) made by cells of *Serratia* sp. pre-grown in lactose limited continuous culture showed nearly twice the  $\text{Eu}^{3+}$  uptake and  $\sim 20\%$  higher  $\text{Sr}^{2+}$  uptake than previously reported values for bio-HA. The small size is suggested to be a major factor determining the improved sorption capacity of  $\text{Eu}^{3+}$  since this (but not  $\text{Sr}^{2+}$ ) localizes at grain boundaries. This study indicates the potential of bio-HA for use in radionuclide remediation, in particular the trivalent actinides. Given the current impetus for recovery of rare earth elements from mine and wastewaters, this approach may also have potential for economic recovery of REE from such sources.

## Acknowledgments

The authors wish to thank Prof. J.I. Langford and Drs T. Rong and J. Deans (Schools of Physics, Metallurgy & Materials Science and Chemistry, University of Birmingham) for assistance with XRD analysis, for calculation of crystal size and for SAD analysis, and Mrs L. Thomkins and Mr P. Whittle for help with electron microscopy.

## Funding

This project was supported by the BBSRC (Grant No. 6/E11940), NERC (Grant Nos. NE/L014076/1 and NE/L012537/1) and EPSRC (Grant No. EP/C548809/1).

## References

- Anonymous. 1992. Powder Diffraction File. Card No. 09-0432. Swarthmore, PA: Joint Committee on Powder Diffraction Standards.
- Beruto TD, Giordani M. 1999. Influence of electromagnetic fields on the microstructure of precipitated calcium phosphate nanometric-grains. *J Euro Ceram Soc* 19:1731–1739.
- Bonthrone KM, Quarmby J, Hewitt CJ, Allan V J, Paterson-Beedle M, Kennedy JK, Macaskie LE. 2000. The effect of the growth medium on the composition and metal binding behavior of the extracellular polymeric material of a metal-accumulating *Citrobacter* sp. *Environ Technol* 21:123–134.
- Dean JA, editor. 1992. Lange's Handbook of Chemistry, 14th Ed., New York: McGraw-Hill.
- Dimovic SD, Smiciklas ID, Sljivic-Ivanovic MZ, Plecas IB, Slavkovic-Beskoski L. 2011. The effect of process parameters on kinetics and mechanisms of  $\text{Co}^{2+}$  removal by bone char. *J Environ Sci Health A Tox Hazard Subst Environ Eng* 46:1558–1569.
- Durucan C, Brown P. 2000.  $\alpha$ -Tricalcium phosphate hydrolysis to hydroxyapatite at and near physiological temperature. *J Mater Sci: Mater Med* 11:365–371.
- Ferris FG, Beveridge TJ. 1984. Binding of a paramagnetic metal cation to *Escherichia coli* K-12 outer membrane vesicles. *FEMS Microbiol Lett* 24:43–46.
- Gabriel CTM, Orton DG, Hollister SJ, Feinberg SE, Halloran JW. 2002. Mechanical and in vivo performance of hydroxyapatite implants with controlled architectures. *Biomaterials* 23:1283–1293.
- Handley-Sidhu S, Renshaw JC, Moriyama S, Stolpe B, Mennan C, Bagheriasl S, Yong P, Stamboulis A, Paterson-Beedle M, Sasaki K, Patrick RAD, Lead JR, Macaskie LE. 2011a. Uptake of  $\text{Sr}^{2+}$  and  $\text{Co}^{2+}$  into biogenic hydroxyapatite: implications for biomineral ion exchange synthesis. *Environ Sci Technol* 45:6985–6990.
- Handley-Sidhu S, Renshaw JC, Yong P, Kerley R, Macaskie LE. 2011b. Nano-crystalline hydroxyapatite bio-mineral for the treatment of strontium from aqueous solutions. *Biotechnol Lett* 33:79–87.
- Handley-Sidhu S, Hriljac JA, Cuthbert MO, Renshaw JC, Patrick RAD, Charnock JM, Stolpe B, Lead JR, Baker S, Macaskie LE. 2014. Bacterially produced calcium phosphate nanobiominerals: sorption capacity, site preferences, and stability of captured radionuclides. *Environ Sci Technol* 48:6891–6898.
- Holliday, K, Handley-Sidhu S, Dardenne K, Renshaw J, Macaskie LE, Walther C, Stumpf T. 2012. A new incorporation mechanism for trivalent actinides into bioapatite: A TRLS and EXAFS study. *Langmuir* 28:3845–3851.
- Jeong BC, Hawes C, Bonthrone KM, Macaskie LE. 1997. Localization of enzymatically enhanced heavy metal accumulation by *Citrobacter* sp. and metal accumulation *in vitro* by liposomes containing entrapped enzyme. *Microbiology* 143:2497–2507.
- Kadurugamuwa JL, Beveridge TJ. 1995. Virulence factors are released from *Pseudomonas aeruginosa* in association with membrane vesicles during normal growth and exposure to gentamicin: a novel mechanism of enzyme secretion. *J. Bacteriol* 177:3998–4008.
- Kameyama T. 1999. Hybrid bioceramics with metals and polymers for better biomaterials. *Bull Mater Sci* 22:641–646.
- Keller L, Dollase WA. 2000. X-ray determination of crystalline hydroxyapatite to amorphous calcium-phosphate ratio in plasma sprayed coatings. *J Biomed Mat Res* 49:244–249.
- Ledo HM, Thackray AC, Jones I P, Marquis PM, Macaskie LE, Sammons RL. 2008. Microstructure and composition of biosynthetically synthesised hydroxyapatite. *J Mater Sci Mater Med* 19:3419–3427.
- Macaskie LE, Bonthrone KM, Yong P, Goddard DT. 2000. Enzymically mediated bioprecipitation of uranium by a *Citrobacter* sp.: a concerted role for exocellular lipopolysaccharide and associated phosphatase in biomineral formation. *Microbiology* 146:1855–1867.
- Macaskie LE, Yong P, Paterson-Beedle M, Thackray AC, Marquis PM, Sammons RL, Nott KP, Hall LD. 2005. A novel non line-of-sight method for coating hydroxyapatite onto the surfaces of support materials by biomineralization. *J Biotechnol* 118:187–200.
- Murray AJ, Singh S, Vavlekas D, Tolley MR, Macaskie LE. 2015. Continuous biocatalytic recovery of neodymium and europium. *RSC Advan* 5:8496–8506.
- Paterson-Beedle M, Macaskie LE, Lee CH, Hriljac JA, Jee KY, Kim WH. 2006. Utilization of a hydrogen uranyl phosphate-based ion exchanger supported on a biofilm for the removal of cobalt, strontium and caesium from aqueous solutions. *Hydrometallurgy* 83:141–145.
- Tomsia AP, Moya JS, Guitian F. 1994. New route for hydroxyapatite coating on Ti-based human implants. *Scripta Metall Material* 31:995–1000.
- Vaz L, Lopes AB, Almeida M. 1999. Porosity control of hydroxyapatite implants. *Journal of Mater Sci: Mater Med* 10:239–242.
- Yeong KCB, Wang J, Ng SC. 2001. Mechanochemical synthesis of nano-crystalline hydroxyapatite from CaO and  $\text{CaHPO}_4$ . *Biomaterials* 22:2705–2712.
- Yong P, Beauregard D, Liu W, Zhang Z, Johns ML, Macaskie LE. 2015. One step bioconversion of waste precious metals into *Serratia* biofilm-immobilized catalyst for Cr(VI) reduction. *Biotechnol Lett*.